Epilayer thickness and strain dependence of Ge(113) surface energies

Daniele Scopece*
L-NESS and Department of Material Science, via R. Cozzi 53, University of Milano-Bicocca, I-20125 Milan, Italy

Matthew J. Beck
Department of Chemical and Materials Engineering, University of Kentucky, Lexington, Kentucky 40506, USA
(Received 20 February 2013; published 19 April 2013)

The stability and growth of three-dimensional (3D) nanostructures in the Ge on Si system is controlled in part by the strain- and overlayer-thickness-dependent surface energies of the crystal facets involved. Here, we use density functional theory (DFT) with local-density approximation calculations to calculate the strain- and thickness-dependent energy of various Ge(113) and Si(113) surface reconstructions. Results of DFT calculations are compared to Tersoff potential calculations to assess the relative importance of stress-strain effects compared to electronic effects not captured by empirical atomistic potentials. We find that the self-interstitial-based 3×2 adatom-dimer-interstitial and 3×2 adatom-interstitial surface reconstructions are stable for Ge overlayer thicknesses from 0 to 4 monolayers and at applied biaxial strains from $\sim -4\%$ to 0%. We leverage calculated surface energies to determine net effective surface energies of various experimentally observed 3D Ge on Si nanostructures.

DOI: 10.1103/PhysRevB.87.155310 PACS number(s): 68.35.Md, 68.47.Fg, 81.15.Aa

I. INTRODUCTION

The increasing application of nanostructured materials has driven increased demand for predictive models of the stability and properties of nanoscale systems. Such models must incorporate both nanoscale and microscale effects and are therefore necessarily multiscale. A common approach to constructing multiscale models leverages atomistic calculations, including quantum-mechanical calculations, of fundamental materials properties to parametrize longer-length-scale finite-element or analytic models of microscale behavior.[1–7]

The Ge on Si heteroepitaxial system has become a prototype for self-assembling nanostructured materials systems and has been subject to extensive computational and experimental analysis for the purpose of constructing predictive multiscale models of nanostructure growth during and following epitaxial layer deposition. Models for the stability and growth of experimentally observed nanoscale three-dimensional (3D) islands typically assess the relative stability of 3D structures in contrast to a biaxially strained planar wetting layer (WL) with the same volume. Such comparisons typically include terms describing (i) the elastic relaxation energy of the 3D island, (ii) the surface energy (SE), γ, of both the exposed facets of the islands and the covered WL, and (iii) the energy of the edges at the intersections of island facets.[8–10]

In some circumstances, the quantitative comparison of computationally predicted stability with experimental observation of 3D nanostructures has allowed the extrapolation of parameters inaccessible to both experiment and calculation, including the estimation of edge energies accounting for the complex atomic-scale edge structures[9,11] and calculation of effective net surface energies of entire islands.[8] Quantitative predictions and comparisons to experiment, though, require calculations of absolute surface energies with consistent levels of accuracy for all relevant facets present in the 3D structures. Hence, detailed and computationally consistent surface energy calculations in the Ge on Si system are required for all facets observed to be present in pyramid, "dome,"[12] and "barn"[13,14] nanostructures. In addition, the availability of sets of directly comparable and quantitatively accurate calculated surface energies would allow the determination of the ground-state shape of nanocrystallites.[15]

In this paper, we report calculations of the strain- and WL-thickness-dependent Ge(113) and Ge on Si(113) surface energies. These calculations extend previous studies of (001), (105), and (1 1 10) surface energies in the Ge on Si system[9] and continue construction of a coherent set of surface energies for use as parameters in multiscale models of the growth and evolution of Ge on Si nanostructures.[1,3,4] We leverage the expanded set of computed surface energies to calculate the total effective surface energy of various experimentally observed 3D Ge on Si structures. To explore the role of both electronic and elastic effects we evaluate the surface energy γ with both density functional theory with local-density approximation (DFT-LDA) pseudopotential calculations and the semiempirical Tersoff potentials.[16,17]

The (113) facet is a major, stable facet of both Si and Ge[18–21] and is of renewed interest due to recent observations of technologically promising structures[22] exhibiting the surface. In addition, the (113) facet has been previously studied as a possible facet relevant in the self-assembly of planar nanowires.[23–25] While previous studies have examined the atomic structure and energetics of the unstrained Ge[24,26–31] and Si[30,31] (113) surfaces, no previous studies have examined the strain-dependent surface structures and energies. The fully strain- and wetting-layer-thickness-dependent properties of the (113) surface are required inputs for multiscale models of the self-assembly of 3D nanostructures (including Ge nanowires on Si[2,23]) in the Ge on Si heteroepitaxial system.

II. METHODS

In order to create a consistent set of surface energies with directly comparable accuracies and calculation settings, we adopt settings and parameters equivalent to those used in

Ref. 9. We adopt the slab supercell approach as in previous studies.[1,2,5–7] Surface energies are calculated using density functional theory as implemented in the commercial plane-wave/pseudopotential code VASP.[32,33] Electron-core interactions are modeled with ultrasoft pseudopotentials (USPP),[34] and exchange and correlation effects are described using the LDA of Ceperley and Alder,[35] as parametrized by Perdew and Zunger.[36] The plane-wave cutoff energy is set to 355 eV, and a repeated slab geometry with vacuum regions between slabs of twice the Si diamond cubic lattice constant is used to extract surface excess energies. Eigenvalues are computed on a Monkhorst-Pack grid of special k points,[37] with atomic positions optimized via a conjugate gradient algorithm and relaxed structures identified when the maximum residual force falls below 5 meV/Å. To yield converged calculations in agreement with previous studies of the (001), (105), and (1 1 10) Ge and Si surfaces, the k-point density is determined for each calculation cell according to the "bulk criterion" defined and justified in Ref. 9. In Tersoff calculations the atomic positions are optimized with a steepest descent algorithm, with a maximum residual force of 10^{-6} eV/Å indicating full relaxation.

Calculation cells are created with the code SLABOS.V01,[38] and a representative ball-and-stick model is shown in Fig. 1(a). All the slabs adopted in this work are symmetric with both surfaces reconstructed and contain 21 bilayers (BLs) free to relax at the top and bottom with 2 BLs fixed in their bulk positions at the middle of the slab [green atoms in Fig. 1(a)]. All (113) slabs are four unit cells thick and contain approximately 520 atoms. The number of layers used here is the same as in Ref. 30, and we choose such large slabs to guarantee convergence with respect to slab thickness. Test calculations with thinner slabs [two (113) units cells] do not differ substantially from results with larger slabs.

The reconstructions we consider are sketched in Fig. 1. In the present study we focus on the most stable reconstructions observed in previous papers.[24,27,39,40] The first structure, referred to here as "P", is made of surface pentagons [Figs. 1(a) and 1(b)] and is the 3×1 (113) reconstruction. Figures 1(c) and 1(d) show the "void" reconstruction[28] (labeled "V" here), where a surface pentagon is missing. Figures 1(e) and 1(f) show the 3×2 adatom-dimer-interstitial reconstruction[31] (referred to here as the "interstitial" or "I" reconstruction). The I reconstruction contains a sixfold coordinated self-interstitial atom within every other surface pentagon (circled in Fig. 1) and has been previously found to be the most stable surface reconstruction for unstrained Si(113).[41] It has also previously been found to be very stable for Ge(113)[31,41] but energetically degenerate with the 3×2 adatom-interstitial containing an interstitial atom in each surface pentagon of the cell [see Figs. 1(g) and 1(h)] and labeled here as "I-2". Both the I and I-2 reconstructions are observed experimentally on unstrained surfaces,[41] and for this reason we study both to determine if applied strain lifts the degeneracy in energy of these two structures. As puckered dimer reconstructions[30] previously proposed for Ge(113) surfaces have been shown to be significantly higher in energy than the surface pentagon-based reconstructions,[30] we do not consider these.

Individual calculations cells contain 524, 514, 526, and 528 atoms in the P, V, I, and I-2 reconstructions, respectively.

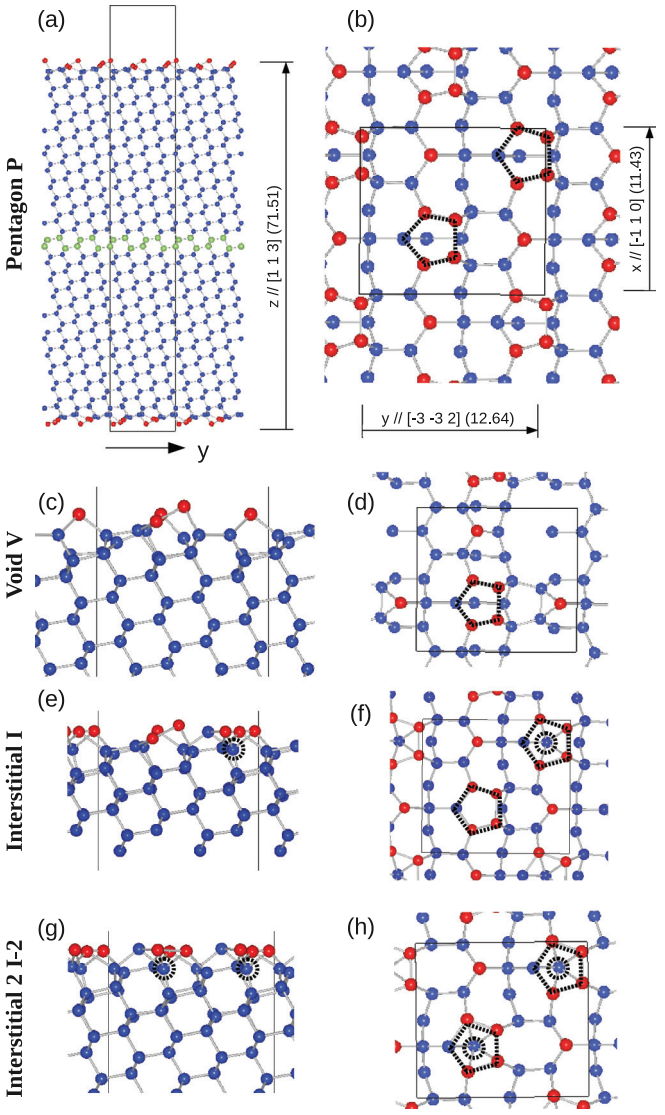

FIG. 1. (Color online) (left) Side and (right) top views of the cells used for the calculations for the reconstructions analyzed. These are the cells used for Ge/Si calculation with coverage of 1.2 ML(001). Ge atoms are red, Si atoms are blue, and fixed Si atoms are green and are placed at the center of the cell. The black solid lines delimit the repeated cells. (a) and (b) report the pentagon "P" reconstruction and show that Ge is placed both at the top and bottom surfaces. In parentheses we write the size of the cell (expressed in Å) along xy in (b) and the thickness of the atoms in (a). (c) and (d) focus on the side view of the top part of the cell and the top view of the void reconstruction. (e) and (f) show the interstitial reconstruction with the interstitial atom highlighted with a dashed circle. (g) and (h) show reconstruction I-2 with two interstitials. In (b), (d), (f), and (h) the pentagons are highlighted with black dashed lines. The plots were made with VESTA software.[56]

Given the cell sizes reported in Figs. 1(a) and 1(b), the bulk criterion for converged k-point density derived in Ref. 9 prescribes a $3 \times 2 \times 1$ k-point mesh for the (113) slabs and yields three irreducible k points. In the present study, however, we adopt a slightly higher density $3 \times 3 \times 1$ k-point mesh giving five irreducible k points. This is done to facilitate a direct comparison to previous calculations of (001), (105),

and (1 1 10) surface energies,[9] as well as to calculations by Stekolnikov *et al.*[31] that use four irreducible k points. Tests reveal that differences in calculated surface energies between the $3 \times 2 \times 1$ mesh prescribed by the bulk criterion and $3 \times 3 \times 1$ meshes used here are only $\sim$0.2–0.3 meV/Å^2.

III. RESULTS AND DISCUSSION

A. Strain dependence of γ_{Ge}

Previous studies have shown that both *unstrained* Si(113) and Ge(113) surfaces are stabilized by surface-incorporated self-interstitials to relieve surface stress.[30,41] The importance of such effects at different strain states is unclear, though, as is as the effect of self-interstitials electronic contributions to the surface energy (SE).

Here we explicitly probe the role of applied strain in determining the absolute surface energy for self-interstitial and noninterstitial Ge(113) surface reconstructions. The SE γ per unit area of the strained surface A_ϵ of a pure Ge slab strained along x and y and free to relax along z is defined in terms of the total energy of the slab E^{tot} as

$$E^{\text{tot}} = \mu_{Ge} N_{Ge} + 2A_\epsilon \gamma. \quad (1)$$

Here, the chemical potential μ_{Ge} is obtained by straining a bulk cell along the x and y directions of the slab and finding the minimum energy per atom as a function of z height.[9]

Following previous works,[9,42] we interpolate the surface energy trend with applied strain using a second-order polynomial:

$$\gamma(\epsilon_{xx},\epsilon_{yy}) = \gamma_0 + \tau_{xx}\epsilon_{xx} + \tau_{yy}\epsilon_{yy} + S_{xx}\epsilon_{xx}^2 + S_{yy}\epsilon_{yy}^2 + S_{xy}\epsilon_{xx}\epsilon_{yy}. \quad (2)$$

In searching for strain-driven transitions between surface reconstructions, we focus on the effect of biaxial strain (i.e., $\epsilon_{xx} = \epsilon_{yy} \equiv \epsilon_{\text{biax}}$). In characterizing the surface energetics of identified stable structures, we consider both biaxial and uniaxial strains ($\epsilon_{xx} \neq \epsilon_{yy}$). Figures 2(a) and 2(b) show surface energy values calculated with the Tersoff potential and DFT-LDA, respectively. Lines show the second-order interpolation given by

$$\gamma(\epsilon_{xx},\epsilon_{yy}) = \gamma_0 + \tau_{\text{biax}}\epsilon_{\text{biax}} + S_{\text{biax}}\epsilon_{\text{biax}}^2. \quad (3)$$

Parameters of this expression found by fitting calculated data are reported in Table I.

Both Tersoff and DFT-calculated results show a single *maximum* in calculated surface energy. These maxima occur at different biaxial strain states, depending on the calculation method employed ($\sim$0% in DFT, ~ -3% in Tersoff). Despite this difference, the existence of a single maximum in γ (ϵ_{biax}), as opposed to multiple maxima, can be deduced as a general rule for strain-dependent surface energies at strains that are not large based on a heuristic elasticity argument.[43]

Looking specifically at the different (113) surface reconstructions, we note that the I and I-2 reconstructions are quite high energy in Tersoff calculations, having higher surface energy than both P and V reconstructions (but, noticeably, still exhibiting lower surface energies than that calculated for unreconstructed "as-cut" slabs, not shown). This is in contrast to DFT results, which find the I and I-2 surface energies to be lower than both P and V surface energies. This contrast can be rationalized by considering that the Tersoff potential accurately treats strain effects[44] but cannot capture electronic or charge transfer effects likely at play in determining the stability of I and I-2 reconstruction,[30,41] where the binding configuration of the interstitial atom(s) differ from that of bulk atoms. Given this, we note that the relatively high surface energy of the I and I-2 reconstructions as calculated with the Tersoff potential does, in fact, support the conclusion that the presence of self-interstitials on (113) surfaces of Ge does *not* primarily stabilize the surface by relieving stress.[41,45] That is, high surface energies for I and I-2 reconstructions in Tersoff calculations suggest that the stability of I and I-2 is due to electronic contributions to surface energy.

In contrast to the divergent results of Tersoff potential and DFT calculations with regards to surface *interstitials*, Fig. 2

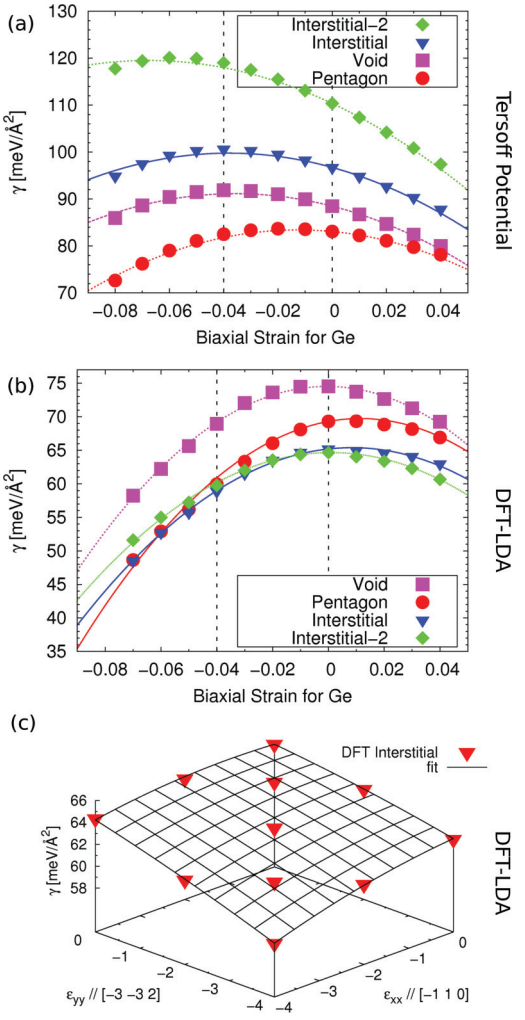

FIG. 2. (Color online) Strain dependence of γ Ge(113) per unit strained surface area (Euler reference frame) in (a) the Tersoff potential and (b) DFT-LDA. Lines are interpolations using Eq. (3), whose parameters are reported in Table I. The vertical dashed lines delimitate the region where the systems Ge_xSi_{1-x}/Si are likely to fall. (c) shows the trend of the interstitial I γ in DFT-LDA along with the interpolation, the parameters of which are reported in Table II. The trend of the uniaxial I-2 reconstruction, showing a similar trend, is not shown here. See Sec. III A for discussion.

TABLE I. Parameters of the biaxial strain dependence of Ge(113) trend reported in Figs. 2(a) and 2(b) interpolated via Eq. (3) for the reconstructions analyzed in this work. Here the strain is expressed in pure numbers (not as a percentage).

Reconstruction	Tersoff	DFT-LDA
Void	$\gamma_0 \simeq 88.48$	74.52
	$\tau_{\text{biax}} \simeq -148.66$	−3.54
	$S_{\text{biax}} \simeq -2080.07$	−3428.88
Pentagon	$\gamma_0 \simeq 83.07$	69.30
	$\tau_{\text{biax}} \simeq -54.42$	76.40
	$S_{\text{biax}} \simeq -2161.08$	−3332.75
Interstitial	$\gamma_0 \simeq 96.72$	65.20
	$\tau_{\text{biax}} \simeq -159.97$	45.84
	$S_{\text{biax}} \simeq -2100.23$	−2734.93
Interstitial 2	$\gamma_0 \simeq 110.36$	64.66
	$\tau_{\text{biax}} \simeq -270.04$	5.35
	$S_{\text{biax}} \simeq -1991.51$	−2655.03

shows that both methods find the P reconstruction to be lower in energy than the V reconstruction. This suggests that elasticity concerns alone are sufficient to favor the formation of surface pentagons. The present results indicate that purely electronic effects are not primary driving forces controlling the relative stability of P and V reconstructions.

Overall, results for Ge(113) surfaces are generally in agreement with previous DFT results[31,41] and show that the Ge(113) is stabilized by self-interstitials [Fig. 2(b)] and that I and I-2 reconstructions have almost degenerate energy. For strained Ge(113) surfaces, the I and I-2 reconstructions remain very similar in energy for a wide range of strains, from −6% to 0%. Therefore, we expect that the coexistence previously predicted[41] for these surface phases likely occurs for both strained and unstrained Ge systems.

Considering now the I and I-2 DFT-calculated surface energies, despite similar energetics overall, the curvature of γ versus strain for the I and I-2 reconstructions is somewhat different. This is highlighted by the fact that the I-2 reconstruction is slightly more stable than the I reconstruction at tensile strains and somewhat less stable for compressive strains. In addition, the strong dependence of the surface energy of the P reconstruction on applied strain results in the P phase as the most stable reconstruction for extremely compressive strains ($\epsilon_{\text{biax}} \sim -6\%$). The mechanisms driving this transformation are unclear, however, and likely represent some combination of strain-related and electronic-structure-related effects.

In order to fully parametrize multiscale models of 3D nanostructure formation we must also have surface energies as a function of uniaxial strain. In this case, we focus solely on the most stable I and I-2 reconstructions and employ only DFT calculations, as Tersoff calculations do not accurately capture all properties of these surfaces. Figure 2(c) shows the results for the I reconstruction as the representative example of the data and the resulting trend obtained through Eq. (2). The I-2 reconstruction exhibits a quantitatively similar trend to that of the I reconstruction and is therefore not shown. Surface energies and surface elastic properties fit from the data for both reconstructions are reported in Table II.

TABLE II. Parameters of Eq. (2) for the trend of $\gamma(113)$ with the uniaxial strain obtained from DFT data for the interstitial (the most stable) reconstructions I and I-2, whose trend is sketched in Fig. 2(c) for reconstruction I. The strain here is for Ge and is expressed as pure numbers (not as a percentage).

Reconstruction	DFT-LDA
Interstitial	$\gamma_0 \simeq 65.20$
	$\tau_{xx} \simeq -26.09$
	$\tau_{yy} \simeq 44.79$
	$S_{xx} \simeq -1255.01$
	$S_{yy} \simeq -547.51$
	$S_{xy} \simeq -1649.00$
Interstitial 2	$\gamma_0 \simeq 64.66$
	$\tau_{xx} \simeq -26.23$
	$\tau_{yy} \simeq 26.12$
	$S_{xx} \simeq -1274.68$
	$S_{yy} \simeq -57.18$
	$S_{xy} \simeq -1685.76$

B. Thickness dependence of γ_{Ge} for Ge on Si(113) epilayers

Analogous to previous calculations,[9] the dependence of γ_{Ge} on epilayer thickness is determined for Si slabs with a fixed number of top and bottom atomic layers converted to Ge [see Fig. 1(a)]. In this case, the surface energy is derived from the total energy of the slab according to

$$E^{\text{tot}} = N_{Ge}\mu_{Ge} + N_{Si}\mu_{Si} + 2A\gamma, \tag{4}$$

where μ_{Si} is the unstrained chemical potential of the N_{Si} atoms of silicon[9] and μ_{Ge} is, as above, the chemical potential of the Poisson-corrected[9] Ge bulk strained at the lattice constant of Si (here $\sim$−5.15885 meV/atom). Figure 3 reports calculated surface energies, with the line representing the interpolation of SE as[9]

$$\gamma(N) = (\gamma_0 - \gamma_\infty)\, e^{-BN} + \gamma_\infty. \tag{5}$$

Here γ_0 is the surface energy of pure, unstrained Si(113), and γ_∞ is the energy of a pure *strained* Ge(113) surface. N is the distance from the topmost (or bottommost, in this case) Ge

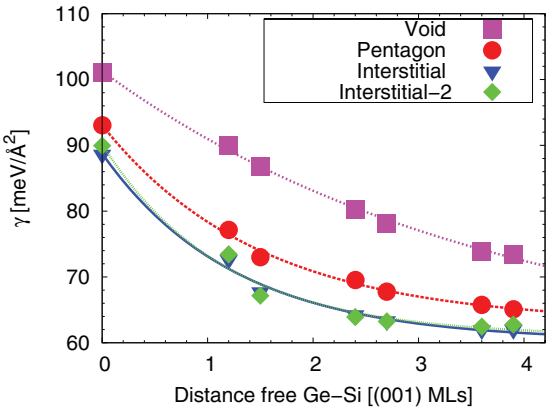

FIG. 3. (Color online) Ge/Si(113) surface energy dependence of the different reconstruction in DFT-LDA. The lines are the interpolation of Eq. (5), whose fitting parameters are reported in Table III. The points group in pairs because of the presence of bilayers. See Sec. III B for discussion.

TABLE III. Parameters of the Ge/Si(113) trend reported in Fig. 3 interpolated via Eq. (5) for the reconstructions analyzed in this work. Here B is in ML^{-1}; γ_0 and γ_∞ in meV/Å^2.

Reconstruction	DFT-LDA
Void	$\gamma_0 \simeq 101.26$ $B \simeq 0.27$ $\gamma_\infty \simeq 57.39$
Pentagon	$\gamma_0 \simeq 93.06$ $B \simeq 0.67$ $\gamma_\infty \simeq 63.00$
Interstitial	$\gamma_0 \simeq 88.75$ $B \simeq 0.80$ $\gamma_\infty \simeq 60.30$
Interstitial 2	$\gamma_0 \simeq 90.14$ $B \simeq 0.87$ $\gamma_\infty \simeq 60.99$

layer to the first Si layer in the bulk expressed in the number of (001) monolayers (MLs). In (113) unit cells 1 ML (001) is equivalent to $\sqrt{11}$ MLs (113).[46] This construction allows direct comparison of the thickness dependence of variously oriented Ge on Si facets. Parameters fit from calculated data are reported in Table III. Figure 3 shows that no surface phase transition should be expected during initial Ge deposition on Si(113) surfaces. That is, the I and I-2 reconstruction are stable for all thicknesses considered [including a "zero" ML surface, which is simply bare Si(113)].[47]

C. Effective surface energy in 3D islands

Combining the above results with previously calculated surface energies of Ge and Ge on Si(001), Si(105), and Si(1 1 10) facets, it is possible to calculate or estimate the total effective surface energy of various experimentally observed 3D structures in the Ge on Si system. Here we specifically calculate net effective surface energies for {105} and {113} pyramids and estimate the net effective surface energy of the experimentally observed "dome" and "barn" nanostructures[48] shown schematically in Fig. 4. Structures with these shapes were constructed using SOWOS.V02.[49] With the aim being to take into account the proper elastic response of the island and to define a general procedure for any island shape, solutions to

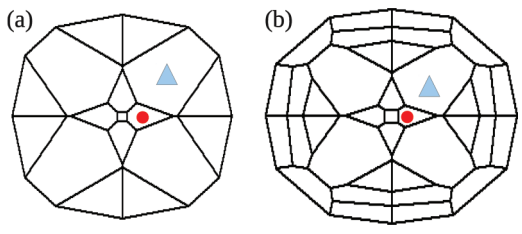

FIG. 4. (Color online) Top view of (a) the dome and (b) barn of Ge used in Ref. 48 and analyzed here in Sec. III C. They are used here as representative examples of the effective strain-dependent surface energies of the (105) (red circles) and (113) (blue triangles) facets. The resulting values of the surface energies are reported in Table IV.

TABLE IV. Effective surface energies of the (105) and (113) facets of pyramids and the domes of Fig. 4. These islands are pure 100% Ge islands laying directly on Si(001), with no WL. Here just the strain dependence of γ is considered, neglecting the dependence on the distance of Ge from the Si substrate. See Sec. III C for discussion. "x" in the table means that the considered facet is not present in the analyzed nanostructure.

Island	$\gamma_{\text{eff}}(105,\epsilon)$ (meV/Å^2)	$\gamma_{\text{eff}}(113,I,\epsilon)$ (meV/Å^2)	$\gamma_{\text{eff}}(113,I-2,\epsilon)$ (meV/Å^2)
{105} Pyr	57.31	x	x
{113} Pyr	x	61.81	62.21
Dome	63.23	62.80	63.07
Barn	64.15	65.03	64.59

the linear elasticity problem were calculated not via approximated analytical expressions, but using finite-element methods (FEM) as implemented in COMSOL MULTIPHYSICS.[50] FEM results provide the strain state present at equilibrium on the surface of the nanostructure, and these strain states, once rotated into the axes of the (113) surface,[51] are used in conjunction with Eq. (2) to determine the surface energy at each point on the nanostructure surface. Total effective surface energies for the four nanostructures considered are tabulated in Table IV.

From these data we note the following points. (i) Changes in the details of strain relaxation due to the specific shape of various island geometries induce changes in the effective surface energies for the same facets on different islands (compare values in each column). (ii) These differences may be on the order of as little as 1 meV/Å^2 [e.g., as for $\gamma_{\text{eff}}(113,I-2,\epsilon)$, comparing the {113} pyramid to dome structures] or as large as $\sim$7 meV/Å^2 [as for $\gamma_{\text{eff}}(105,\epsilon)$, comparing the {105} pyramid to barn structures]. (iii) The effective surface energy is smallest for {105} pyramids, highlighting the relative stability of the {105} facet compared to other major facets in the Ge on Si system (a point confirmed experimentally[52,53]), as well as the importance of strain relaxation (that is, reduction in elastic energy) in driving the evolution of nanostructure shapes from {105} pyramids to "domes" and subsequently "barns" with increasing nanostructure volume. (iv) Considering only the {105} and {113} facets [as surface energy has not previously been calculated for the (15 3 23) facet], we estimate a net effective surface energy for dome structures of $\sim$63 meV/Å^2, close to the experimentally derived estimate of 65 meV/Å^2 reported in Ref. 8. A more definite confirmation of this estimate will come when calculations of strain- and thickness-dependent surface energies are extended to the (15 3 23) facet.

Expanding on these points, we note that points (i) and (ii) above demonstrate that the surface energies of facets on heteroepitaxial nanoislands cannot accurately be treated as fixed, single values. In turn this necessarily implies that multiscale models merging atomistically calculated, strain- and thickness-dependent surface energies with FEM or continuum-calculated elastic properties are required to accurately compute the formation energy and relative stability of faceted nanostructures. In addition, the stability of facets on strained nanoislands cannot be directly extracted from a simple geometrical analysis analogous to a Wulff construction.[54,55]

The present calculations of net effective surface energy limit the complexity compared to that of the real system by neglecting WL thickness and intermixing effects. These simplifications have been previously addressed for 105 surface ripples and are not expected to affect the trends reported here. In addition, it should be noted that for sufficiently small nanostructures, where facet sizes are on the order of or smaller than the surface unit cell, facet surface energies are expected to differ from those calculated for ideal facets. Finally, assuming nanostructures with sufficiently large facets, we note that the present multiscale model for calculation of effective surface energy is generally applicable to any materials system and structure geometry for which strain- and thickness-dependent surface energies, in combination with bulk elastic properties, are known. This, of course, includes other more complex Ge on Si island-substrate geometries.

IV. CONCLUSIONS

We have calculated the strain- and thickness-dependent surface energy of the Ge(113) and Ge on Si(113) surfaces. Calculated values are consistent with previous studies and show that neither strain nor overlayer thickness significantly affects the relative stability of various candidate surface reconstructions. Surface energies have been calculated with the same calculation settings and convergence parameters used in previous studies of (001), (105), and (1 1 10) surfaces, allowing quantitatively consistent multiscale calculations of net effective surface energy for a range of experimentally observed 3D Ge on Si nanostructures. As noted previously,[9] Tersoff potential results differ from DFT results due to electronic effects on surface energies that are not captured by the Tersoff potential. Finally, in combination with previous results for (1 1 10) nanoripples,[9] we note that stable reconstructions of experimentally observed facets all exhibit similar absolute surface energies (∼60–70 meV/Å^2), making the details of their strain and thickness dependence critical in determining relative facet stability and therefore the energetics and shapes of 3D nanostructures.

APPENDIX: INPUT FILES FOR THE ISLANDS

Here we report the input code for SOWOS[49] to create the pyramids and the islands depicted in Fig. 4 and whose effective surface energies are reported in Table IV.

Pyramid 105:

```
2
B  0 0 1   w  0.0   x 1
S  1 0 5   w 10.0   x 0
```

Pyramid 113:

```
2
B  0 0 1   w  0.0   x 1
S  1 1 3   w 10.0   x 0
```

Dome:

```
5
B   0  0  1   w  0.0   x 1
S   1  0  5   w  9.2   x 0
S   1  1  3   w  9.7   x 0
S  15  3 23   w 11.8   x 0
S   0  0  1   w  9.2   x 1
```

Barn:

```
8
B   0  0  1   w  0.0   x 1
S   1  0  5   w  9.2   x 0
S   1  1  3   w  9.2   x 0
S  15  3 23   w 10.2   x 0
S   0  0  1   w  9.2   x 1
S   1  1  1   w 13.0   x 0
S  20  4 23   w 11.0   x 0
S  23  4 20   w 12.0   x 0
```

*Present address: EMPA, Swiss Federal Laboratories for Materials Science and Technology, Überlandstrasse 129, CH-8600 Dübendorf, Switzerland; group nanotech@surfaces; daniele.scopece@mater.unimib.it; daniele.scopece.science@gmail.com

[1]G.-H. Lu and F. Liu, Phys. Rev. Lett. **94**, 176103 (2005).
[2]G.-H. Lu, M. Cuma, and F. Liu, Phys. Rev. B **72**, 125415 (2005).
[3]H. Hu, H. Gao, and F. Liu, Phys. Rev. Lett. **109**, 106103 (2012).
[4]N. Moll, M. Scheffler, and E. Pehlke, Phys. Rev. B **58**, 4566 (1998).
[5]O. Shklyaev, M. J. Beck, M. Asta, M. Miksis, and P. Voorhees, Phys. Rev. Lett. **94**, 176102 (2005).
[6]L. G. Wang, P. Kratzer, M. Scheffler, and N. Moll, Phys. Rev. Lett. **82**, 4042 (1999).
[7]P. Kratzer and M. Scheffler, Comput. Sci. Eng. **3**, 16 (2001).
[8]M. Brehm, F. Montalenti, M. Grydlik, G. Vastola, H. Lichtenberger, N. Hrauda, M. J. Beck, T. Fromherz, F. Schäffler, L. Miglio, and G. Bauer, Phys. Rev. B **80**, 205321 (2009).
[9]D. Scopece, F. Montalenti, and M. J. Beck, Phys. Rev. B **85**, 085312 (2012).
[10]E. Pehlke, N. Moll, and A. Kley, Appl. Phys. A **534**, 525 (1997).
[11]G. Chen, B. Sanduijav, D. Matei, G. Springholz, D. Scopece, M. J. Beck, F. Montalenti, and L. Miglio, Phys. Rev. Lett. **108**, 055503 (2012).
[12]A. Rastelli and H. von Känel, Surf. Sci. Lett. **515**, L493 (2002).
[13]M. Stoffel, A. Rastelli, J. Tersoff, T. Merdzhanova, and O. G. Schmidt, Phys. Rev. B **74**, 155326 (2006).
[14]A. Rastelli, M. Stoffel, G. Katsaros, J. Tersoff, U. Denker, T. Merdzhanova, G. Kar, G. Costantini, K. Kern, H. von Kanel, and O. G. Schmidt, Microelectron. J. **37**, 1471 (2006)
[15]A. A. Stekolnikov and F. Bechstedt, Phys. Rev. B **72**, 125326 (2005).
[16]J. Tersoff, Phys. Rev. B **39**, 5566 (1989).
[17]J. Tersoff, Phys. Rev. B **41**, 3248 (1990).
[18]Z. Gai, R. G. Zhao, W. Li, Y. Fujikawa, T. Sakurai, and W. S. Yang, Phys. Rev. B **64**, 125201 (2001).
[19]Z. Gai, W. Yang, R. G. Zhao, and T. Sakurai, Phys. Rev. B **59**, 15230 (1999).

[20]Z. Gai, H. Ji, B. Gao, R. G. Zhao, and W. S. Yang, Phys. Rev. B **54**, 8593 (1996).
[21]Z. Gai, R. G. Zhao, X. Li, and W. S. Yang, Phys. Rev. B **58**, 4572 (1998).
[22]C. V. Falub, H. von Kanel, F. Isa, R. Bergamaschini, A. Marzegalli, D. Chrastina, G. Isella, E. Muller, P. Niedermann, and L. Miglio, Science **335**, 1330 (2012).
[23]H. Omi and T. Ogino, Appl. Phys. Lett. **71**, 2163 (1997).
[24]G. P. Srivastava, Rep. Prog. Phys. **60**, 561 (1997).
[25]T. Clausen, T. Schmidt, J. I. Flege, and A. Locatelli, Appl. Surf. Sci. **252**, 5321 (2006).
[26]D. Bird, L. Clarke, R. King-Smith, M. Payne, I. Stich, and A. P. Sutton, Phys. Rev. Lett. **69**, 3785 (1992).
[27]J. Dabrowski, H.-J. Mussig, and G. Wolff, Phys. Rev. Lett. **73**, 1660 (1994).
[28]J. Dabrowski, H.-J. Mussig, and G. Wolff, Surf. Sci. **331**, 1022 (1995).
[29]J. Knall, J. B. Pethica, J. Todd, and J. Wilson, Phys. Rev. Lett. **66**, 1733 (1991).
[30]A. A. Stekolnikov, J. Furthmüller, and F. Bechstedt, Phys. Rev. B **67**, 195332 (2003).
[31]A. A. Stekolnikov, J. Furthmüller, and F. Bechstedt, Phys. Rev. B **68**, 205306 (2003).
[32]G. Kresse and J. Furthmüller, Phys. Rev. B **54**, 11169 (1996).
[33]G. Kresse and J. Furthmüller, Comput. Mater. Sci. **6**, 15 (1996).
[34]D. Vanderbilt, Phys. Rev. B **41**, 7892 (1990).
[35]D. M. Ceperley and B. J. Alder, Phys. Rev. Lett. **45**, 566 (1980).
[36]J. P. Perdew and A. Zunger, Phys. Rev. B **23**, 5048 (1981).
[37]H. J. Monkhorst and J. D. Pack, Phys. Rev. B **13**, 5188 (1976).
[38]D. Scopece (unpublished); http://www.danielescopece84.altervista.org/slabos.html.
[39]J. Schreiner, K. Jacobi, and W. Selke, Phys. Rev. B **49**, 2706 (1994).
[40]K. A. Feng, X. M. Hu, Z. Lin, and Y. R. Xing, Appl. Surf. Sci. **120**, 94 (1997).
[41]A. Laracuente, S. Erwin, and L. Whitman, Phys. Rev. Lett. **81**, 5177 (1998).
[42]M. J. Beck, Ph.D. thesis, Northwestern University, Evanston, Illinois, 2005.
[43]This will be discussed in a future manuscript.
[44]D. Srivastava, R. S. Taylor, and B. J. Garrison, J. Vac. Sci. Technol. B **9**, 1517 (1991).
[45]H. Vogler, A. Iglesias, W. Moritz, and H. Over, Phys. Rev. B **57**, 2315 (1998).
[46]This will be proven in a future manuscript.
[47]Our data for unstrained Si(113) surface energy have a negligible discrepancy from the ones from Stekolnikov *et al*. (Ref. 30) and a small one (given probably by the different settings of the calculations) from the ones of Laracuente *et al*. (Ref. 41).
[48]J. J. Zhang, F. Montalenti, A. Rastelli, N. Hrauda, D. Scopece, H. Groiss, J. Stangl, F. Pezzoli, F. Schäffler, O. G. Schmidt, L. Miglio, and G. Bauer, Phys. Rev. Lett. **105**, 166102 (2010).
[49]D. Scopece, J. Appl. Crystallogr. **46** (2013), http://www.danielescopece84.altervista.org/sowos.html.
[50]COMSOL Inc., COMSOL MULTIPHYSICS user's guide, http://www.comsol.com.
[51]T. Hammerschmidt, P. Kratzer, and M. Scheffler, Phys. Rev. B **75**, 235328 (2007).
[52]J. Zhang, G. Katsaros, F. Montalenti, D. Scopece, R. Rezaev, C. Mickel, B. Rellinghaus, L. Miglio, S. DeFranceschi, A. Rastelli, and O. Schmidt, Phys. Rev. Lett. **109**, 085502 (2012).
[53]J. J. Zhang, A. Rastelli, O. G. Schmidt, D. Scopece, L. Miglio, and F. Montalenti (unpublished).
[54]C. Rottman and M. Wortis, Phys. Rep. **103**, 59 (1984).
[55]H. Bonzel and M. Nowicki, Phys. Rev. B **70**, 245430 (2004).
[56]K. Momma and F. Izumi, J. Appl. Crystallogr. **41**, 653 (2008).